Diffusive instabilities in heterogeneous systems

Vladimir K. Vanag and Irving R. Epstein
Department of Chemistry and Volen Center for Complex Systems, MS 015, Brandeis University, Waltham, Massachusetts 02454-9110

(Received 8 May 2003; accepted 16 July 2003)

We investigate the behavior of a system composed of two small identical water droplets loaded with an activator-inhibitor system possessing only a single stable steady state and coupled through a third, ''signaling'' species able to diffuse through the interdroplet medium. Depending on whether the third species is coupled to the activator or the inhibitor, the system can exhibit wave instability, which is equivalent to out-of-phase oscillations, or Turing instability, which is equivalent to the birth of two new stationary steady states. For a large interdroplet gap, equivalent to a large time delay, droplets can undergo synchronous, in-phase oscillations. Our analysis can be extended to a system of many coupled in-line droplets, as we illustrate. © *2003 American Institute of Physics.*
[DOI: 10.1063/1.1606677]

I. INTRODUCTION

The recent discoveries of Turing patterns, antispirals, standing and packet waves in the Belousov–Zhabotinsky (BZ) reaction dispersed in aerosol OT (AOT) water-in-oil microemulsions[1–3] call for a deeper understanding of the nature of diffusive instabilities in heterogeneous media. In his seminal paper,[4] Turing predicted two types of diffusive instabilities in homogeneous media, one of which (now generally known as the Turing instability) generates stationary patterns that are periodic in space, while the other (sometimes called the finite wavelength or oscillatory Turing instability, and referred to here as the wave instability, though no universally accepted terminology has yet emerged) produces patterns periodic both in time and in space. For the Turing instability, an eigenvalue Λ of the Jacobian matrix evaluated at a stationary state of the system is real and has a positive maximum at wave number $k_0>0$. For the wave instability, a complex eigenvalue has positive real part $\mathrm{Re}(\Lambda)$ for some range of k and exhibits a maximum of $\mathrm{Re}(\Lambda)$ at some finite k_0. The characteristic wavelength of Turing patterns or waves (traveling or standing), λ_0 is equal to $2\pi/k_0$ (note that the wave instability can also produce trigger waves, in which case the wavelength λ_0, has a different form[5]).

In analyzing reaction-diffusion media, Turing explored two mathematical approaches: continuous and discrete.[4] In the latter case, the medium was described as a set of ''small reactors'' connected through mass exchange terms like $k_{ex}(u_{n-1}+u_{n+1}-2u_n)$, where u is the concentration of some species (a ''morphogen'' in Turing's terminology) and n is the reactor index. The two lines of attack have given rise to two scientific directions: ''pattern formation'' and ''coupled oscillators.'' Both of these approaches play important roles in biology and other branches of science where nonlinear processes and complex behavior are found. However, despite occasional allusions to their similarity,[6,7] these two directions have developed nearly independently of one other. We shall show that both of these approaches are useful for analyzing heterogeneous systems and shall comment on how they overlap.

Smale[7] was probably the first to apply Turing's methodology to the problem of diffusive coupling between two identical cells. Using a coupling term of the form $k_{ex}(z_1-z_2)$, where z_1 and z_2 represent concentrations in the two cells, he showed that cells with a single stable steady state (SS) can oscillate as a result of the coupling, a phenomenon now known as rhythmogenesis. Almost all subsequent works on ''coupled cells'' or ''coupled oscillators'' have used this coupling term, thus ignoring the intercellular space, which is always present.

In this paper, we consider a simple, heterogeneous, one-dimensional system consisting of two identical reactors and a gap between them (Fig. 1). We may think of these reactors as living cells or water droplets in a microemulsion (where the gap is an oil). Unlike AOT microemulsions, which have nanometer-size droplets, we consider larger droplets with a size l_R comparable to or smaller than typical experimentally observed wavelengths λ_0, which are in the range 10–200 μm.[1,8] Each reactor contains an activator (u), an inhibitor (ν), and a third species w that is linearly coupled either with u or with ν. In the reactors, the three species have identical diffusion coefficients, $D_u=D_\nu=D_w$. Only species w can diffuse into the gap, within which $D_u=D_\nu=u=\nu=0$. Thus the two reactors communicate with each other only by means of the ''signaling'' molecules w.

Two parameters typically play major roles in determining the behavior of coupled systems: the coupling strength and the time delay associated with transfer between subsystems. The importance of delay was demonstrated recently in investigations of ''phase death'' or ''amplitude death,'' i.e., the cessation of oscillations when two identical oscillators are coupled with a moderate delay.[9–11] An analogous result was obtained some time ago for coupled chemical oscillators.[12,13] In that work, a controllable time delay τ was deliberately introduced into the experimental configuration and was explicitly included in the model equations. Holz and Schneider[12] also produced rhythmogenesis by coupling two

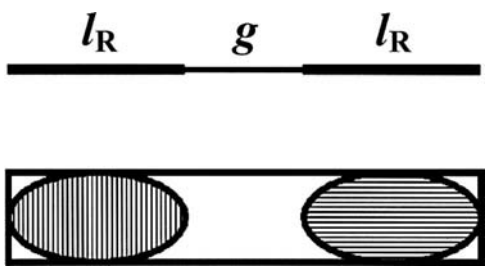

FIG. 1. Heterogeneous system of two droplets (reactors) and a gap.

identical SS's with a time delay. Without a delay, two identical SS's cannot produce in-phase (synchronous) oscillations.[14] With time delay, in-phase oscillations were obtained.[12] The effect of time delay (and coupling strength) on excitation circulating over coupled cells has also been studied.[15] In our system, time delay is introduced through the diffusion of species w across the gap.

To gain insight into the behavior of the system in Fig. 1, we apply both the continuous and the discrete approaches. Before tackling the full system, we explore the behavior of two approximate representations. In the first (system A), we take the pattern formation approach, and consider a one-dimensional system in which the effects of separation into drops and a gap are replaced by a redefinition of the diffusion coefficients. The second model (system B) employs the coupling point of view and replaces the full system by two coupled zero-dimensional (well-mixed reactor) subsystems. We (i) carry out a linear stability analysis of the partial differential equations (PDE's) for system A and of the ordinary differential equations (ODE's) for system B; (ii) solve the algebraic equations for the steady states of system B, which may differ from the single steady state of the isolated uncoupled reactor; and (iii) numerically integrate the PDE's for the full heterogeneous system as well as the equations for the approximate systems. These approaches will allow us not only to understand the system behavior better, but also to draw together the languages and terminology of ''pattern formation'' and ''coupled oscillators'' to enrich our understanding of Turing patterns, wave instability, rhythmogenesis, out-of-phase and in-phase oscillations. We demonstrate that patterning and coupling have much in common, especially if we are interested in identical ''small reactors'' confined to a region comparable in extent with the characteristic pattern's wavelength λ_0. We are investigating rhythmogenesis and patterning in two coupled identical spatially extended subsystems, each of which possesses a single steady state when alone. We therefore refer to ''coupled cells (or reactors)'' rather than ''coupled oscillators,'' since our subsystems do not exhibit bulk oscillations [$\mathrm{Re}(\Lambda)<0$ at $k=0$].

In Secs. II and III we consider two cases, when the signaling molecule w is coupled only with the inhibitor ν or only with the activator u, respectively. Some investigations, notably those of Stolyarov *et al.*,[16] have stressed that the result of coupling depends upon the nature of the variable, ''fast'' or ''slow,'' by which the two subsystems are coupled. In this paper we shift emphasis and point out that the outcome of coupling is determined largely by whether it is the activator or the inhibitor variable through which the coupling occurs, regardless of the time scale on which these variables change.

II. COUPLING THROUGH THE INHIBITOR: TURING INSTABILITY

Our system, shown in Fig. 1, has total length

$$L=2l_R+g \tag{1}$$

and zero-flux boundary conditions at its ends. In the case of interaction between the inhibitor and the signaling species, each reactor droplet may be described by the following equations:

$$\partial u/\partial t=f(u,\nu)+D_u\partial^2 u/\partial x^2, \tag{2}$$

$$\partial \nu/\partial t=g(u,\nu)-c\nu+dw+D_v\partial^2 \nu/\partial x^2, \tag{3}$$

$$\partial w/\partial t=c\nu-dw+D_w\partial^2 w/\partial x^2, \tag{4}$$

where c and d are positive constants.

To be more specific, most of our numerical simulations employ the abstract Brusselator model,[17] with

$$f(u,\nu)=a-(1+b)u+u^2\nu, \tag{5}$$

$$g(u,\nu)=bu-u^2\nu, \tag{6}$$

though other, more chemically relevant functions $f(u,\nu)$ and $g(u,\nu)$ may be chosen, for example, the Lengyel–Epstein model[18] for the chlorine dioxide-iodine-malonic acid reaction or the Oregonator model for the BZ reaction.[19] It has been shown previously[16] for two coupled identical oscillators that the results of coupling are largely independent of the details of the chemical system, i.e., the functions $f(u,\nu)$ and $g(u,\nu)$, if those functions satisfy some basic requirements for activator-inhibitor systems with positive and negative feedbacks.

A. Linear stability analysis: PDE—homogeneous system A-I

Our first step is to construct a homogeneous system that mimics the behavior of our full heterogeneous system, including the gap. We can then apply standard linear stability analysis to the corresponding PDE's to calculate where the most positive eigenvalue passes through zero and where its real part reaches a maximum. This analysis will permit us to find a range of g where the system exhibits interesting behavior. Species u and ν cannot diffuse through the gap, i.e., no molecules of u or ν from the left reactor can reach the right reactor and vice versa. To obtain our homogeneous approximation, in which there is no difference between the reactor and the gap, we therefore set the diffusivities of u and ν to zero, despite the fact that they do diffuse inside the actual droplets. Thus we put $D_u=D_v=0$ and $D_w\neq 0$ in Eqs. (2)–(4) and study these equations in a homogeneous system of length $L=2l_R+g$, which we refer to as system A-I. Later, we shall verify this approach by comparison with simulations of the full heterogeneous model.

Under these assumptions, the characteristic equation in general form is

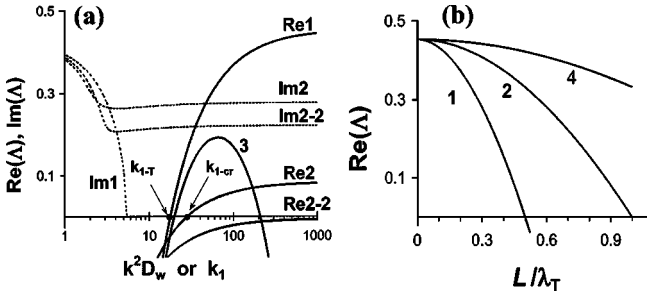

FIG. 2. (a) Dispersion curves for systems A-I and B-I and Brusselator model with $a=3.06$, $b=7$, $c=2$, $d=5$. Abscissa shows k^2D_w for system A-I, k_1 for system B-I. $D_w=100$, $D_v=0$, $D_u=$(Re1) 0, (curve 3) 0.1. Im $=\mathrm{Im}(\Lambda)/5$. Curves Re1 and 3 are independent of r. Re2 (Re2-2) and Im2 (Im2-2) are obtained at $r=0.1$ (0.19). When Re1$=0$, $k\equiv k_{\min}=0.421\,31$ and $k_1\equiv k_{1-T}=17.77$. When Re2$=0$, $k_1=k_{1-\mathrm{cr}}$. For curve Re2-2, Re(Λ) is negative at any k_1. (b) System A. Transformed curve Re1 in (a) for $k=m\pi/L$, $\lambda_T=2\pi/k_{\min}=14.91$, modes $m=1$, 2, 4.

$$\begin{vmatrix} f_u-\Lambda & f_v & 0 \\ g_u & g_v-c-\Lambda & d \\ 0 & c & -d-\Lambda-k^2D_w \end{vmatrix} = D_0-k^2D_wD_1=0, \tag{7}$$

where

$$D_0=(f_u-\Lambda)(g_v-c-\Lambda)(-d-\Lambda)-cd(f_u-\Lambda) - f_vg_u(-d-\Lambda), \tag{8}$$

$$D_1=(f_u-\Lambda)(g_v-c-\Lambda)-f_vg_u, \tag{9}$$

and f_u, f_v, g_u, g_v are the partial derivatives of $f(u,\nu)$ and $g(u,\nu)$ with respect to u and ν, respectively. For the Brusselator model, the steady states are $u_{\mathrm{SS}}=a$, $\nu_{\mathrm{SS}}=b/a$, and $w_{\mathrm{SS}}=cb/(ad)$, and a typical dispersion curve is presented in Fig. 2(a) as (Re1, Im1). We see that Re$(\Lambda)\geqslant 0$ and Im$(\Lambda)=0$ for wave numbers $k\geqslant k_{\min}$ ($k_{\min}$ is denoted as k_{1-T}), i.e., we have a Turing instability. This result implies that, if our homogeneous approach with $D_u=D_v=0$ is valid, Turing instability can arise in heterogeneous systems like those shown in Fig. 1 even with equal diffusion coefficients of all species in the droplets. Earlier, Turing-like patterns with equal diffusion coefficients were predicted for homogeneous systems with flow (convective) terms[20,21] or for finite perturbations (subcritical Turing bifurcation),[22] as well as for heterogeneous systems with special conditions like anomalous diffusion.

For $D_u=D_v=0$, Re(Λ) does not have a maximum, but rather a plateau as $k\to\infty$. To obtain a maximum, D_u must be positive. A dispersion curve for small but nonzero D_u is shown in Fig. 2(a) as curve 3. Since the system length L is comparable with λ_0, it is useful to present dispersion curves as a function of L, replacing the wave number k by $m\pi/L$. The dependence of Re(Λ) on L for the modes $m=1$ (half a wavelength), $m=2$ (one wavelength), and $m=4$ (two wavelengths) are shown in Fig. 2(b). As the characteristic wavelength we chose $\lambda_T=2\pi/k_{\min}$. If $L>0.5\lambda_T$, Turing structures with half a wavelength ($m=1$) become unstable [Re$(\Lambda)<0$]. More generally, the mth mode becomes unstable when $L>m\lambda_T/2$. For our case of two coupled "small reactors," the $m=1$ Turing structure has one reactor in a steady state above and the other in a steady state below the homogeneous steady state (u_{SS}). We show later how to find these new steady states, which correspond to the maxima and minima of the Turing patterns in the corresponding systems of infinite length.

B. Linear stability analysis: Coupled ODE: System B-I

Since the reactors (or droplets) and the gap are quite small, we now make the approximation that each is perfectly homogeneous due to diffusive mixing and represent the effects of the gap linking the two droplets by the geometric parameter

$$r=l_R/g \tag{10}$$

and phenomenological rate constants k_1 and k_2 that characterize the coupling between the reactors via w. Under these conditions, system B-I in the geometry shown in Fig. 1 (three coupled in-line reactors) is described by the following ODE's:

$$du_1/dt=f(u_1,\nu_1), \tag{11}$$

$$d\nu_1/dt=g(u_1,\nu_1)-c\nu_1+dw_1, \tag{12}$$

$$dw_1/dt=c\nu_1-dw_1-k_1w_1+k_2w_3/r, \tag{13}$$

$$dw_3/dt=-2k_2w_3+rk_1(w_1+w_2), \tag{14}$$

$$du_2/dt=f(u_2,\nu_2), \tag{15}$$

$$d\nu_2/dt=g(u_2,\nu_2)-c\nu_2+dw_2, \tag{16}$$

$$dw_2/dt=c\nu_2-dw_2-k_1w_2+k_2w_3/r. \tag{17}$$

Subscripts 1 and 2 refer to subsystems (drops) 1 and 2, respectively, while subscript 3 refers to the gap. The terms k_2w_3/r, $-k_1w_1$, and $-k_1w_2$ in Eqs. (13) and (17) and all terms in Eq. (14) describe the rates of mass transfer between adjacent reactors (gap and two droplets) of different volumes (proportional to the lengths l_R and g).

In Eqs. (11)–(17), we may view k_1 as the coupling strength and k_2 as inversely correlated with the time delay for communication, mediated by w, between the reactors. The parameters k_1 and k_2, however, are not independent of one another, and are related by the volume ratio r and the partition coefficient P of w between the reactor and the gap. The partition coefficient, which depends upon the thermodynamic properties of w and the solvents in the reactors and the gap, gives the equilibrium ratio of concentrations, $P\equiv w_{1s}/w_{3s}=w_{2s}/w_{3s}$, in the absence of reaction (transport only), where the subscript s denotes steady state. Substituting these expressions for P into Eq. (14) at steady state, when $dw_3/dt=0$, yields

$$k_2=Prk_1 \tag{18}$$

which suggests, as intuition implies, that the time delay should increase with the size of the gap and decrease with k_1P, i.e., with the relative ease with which w moves between the two reactors. Note that Eq. (18) simply expresses the

relation between rate constants k_1 and k_2 and the equilibrium ratio P. Substituting Eq. (18) into Eqs. (13), (14), and (17), we obtain

$$dw_1/dt = c\nu_1 - dw_1 - k_1(w_1 - Pw_3), \tag{13'}$$

$$dPw_3/dt = -Prk_1(2Pw_3 - w_1 - w_2), \tag{14'}$$

$$dw_2/dt = c\nu_2 - dw_2 - k_1(w_2 - Pw_3). \tag{17'}$$

To simplify the form of the equations, we can introduce a new variable $w_3' = Pw_3$ and a new parameter $g' = g/P$ (or $r' = Pr$), or simply put $P = 1$ without loss of generality. We will refer to system (11, 12, 13′, 14′, 15, 16, 17′) with $P = 1$ as system B-I. The coupling constant k_1 and the ratio $r = l_R/g$ can be considered as the two independent parameters that govern this system.

Linear stability analysis of system B-I gives the following characteristic equation:

$$(D_0 - k_1 D_1)(2k_1 r D_0 + \Lambda D_0 - \Lambda k_1 D_1) = 0, \tag{19}$$

where D_0 and D_1 are the same as in Eq. (7). Comparing Eqs. (7) and (19), we write

$$k_1 = k^2 D_w. \tag{20}$$

The wave number k is related to the total system length $L = 2l_R + g$. Approximately, $k \cong \pi/L$. Later we shall show that L in this relation must be modified slightly if $g \gg l_R$. Note that for large systems with $L \gg \lambda_0$, the characteristic wavelength, λ_0, is essentially independent of the system length L, while in our case, where $L \leqslant \lambda_0$, the system length plays the role of the characteristic wavelength. Equation (20) provides an important relationship, which we shall employ later, for linking systems A-I and B-I. By combining Eqs. (18) and (20) with $k \cong \pi/L$, we can express k_2^{-1}, the time delay caused by w, in terms of D_w, P and the geometry of the system as $k_2^{-1} \cong (2l_R + g)^2 g/(\pi^2 P l_R D_w)$.

Since Eq. (19) contains two factors, we now have additional roots (eigenvalues), which may lead to additional instabilities. The first term $(D_0 - k_1 D_1)$, which is independent of r, gives the same eigenvalues as Eq. (7). A second eigenvalue with positive real part originates from the second factor in Eq. (19), $(2k_1 r D_0 + \Lambda D_0 - \Lambda k_1 D_1)$, and depends on r. Its real and imaginary parts (with Brusselator kinetics) are shown as Re2 and Im2, respectively, in Fig. 2(a). We see that Im2$\neq$0, when Re2$>$0, implying that the system can oscillate when Re2$>$0. However, since for positive Re1 and Re2, Re1$>$Re2 at all k_1 and r, oscillations will not necessarily be found. If the mode with larger Re(Λ) dominates, then only the stationary half wavelength Turing structure will emerge. We test the system's behavior numerically below. The dependence of the critical value of k_1, $k_{1-\mathrm{cr}}$, at which Re2$=$0 [Fig. 2(a)], on r is shown as curve 2 in Fig. 4(a). The value of r at which Re2(Λ) becomes negative at any k_1 can be found analytically from the cubic equation $2rD_0 - \Lambda D_1 = 0$. Typical examples of such dispersion curves are shown in Fig. 2(a) as curves Re2-2 and Im2-2. If $r \to 0$, then $k_{1-\mathrm{cr}} \to k_{1-T}$. For k_1 such that $k_{1-T} < k_1 < k_{1-\mathrm{cr}}$, only stationary patterns occur.

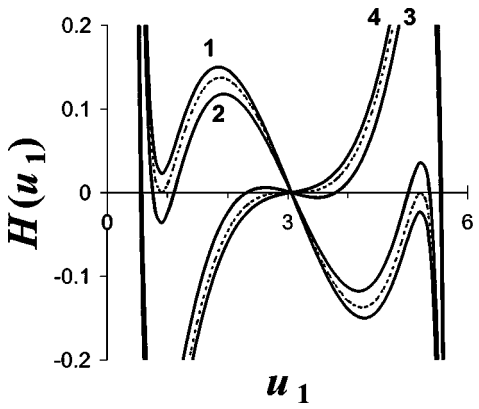

FIG. 3. Function $H(u_1)$, whose zeros give the steady states of system B-I, plotted for several k_1. $k_1 = (1)$ 6.8, (2) 7.5, (3) 15, (4) 20; $a = 3.06$, $b = 7$, $c = 2$, $d = 5$. Local minimum and local maximum of the dotted curve ($k_1 = k_{1-\mathrm{ST}} = 7.05$) lying between curves 1 and 2 are tangent to the abscissa. $k_{1-T} = 17.77$ is the value of k_1 at which system B-I goes from having three roots to five and $dH/du_1 = 0$ at $u_1 = u_{\mathrm{SS}} = a$ (dotted curve between curves 3 and 4).

C. Steady states: ODE

In addition to the homogeneous steady state corresponding to the SS's of the uncoupled subsystems, system B-I may have additional, inhomogeneous steady states. With some algebraic manipulation, after setting all the rates to zero, we can eliminate the w_i, solve $f(u,\nu) = 0$ for ν_{1s} and ν_{2s} as functions of u_{1s} and u_{2s}, respectively, find the relationship

$$\nu_{2s} = \nu_{1s} - 2(1 + d/k_1) g(u_{1s}, \nu_{1s})/c,$$

and finally substitute all these results into

$$g(u_{1s}, \nu_{1s}) = -g(u_{2s}, \nu_{2s}). \tag{21}$$

Equation (21) allows us to obtain a single algebraic equation in u_1, which may be solved, numerically if necessary, for the steady states.

For the Brusselator model, Eq. (21) gives

$$a - u_{1s} = -bu_{2s} + u_{2s}^2 \nu_{2s}, \tag{22}$$

where $\nu_{2s} = \nu_{1s} - 2(1 + d/k_1)(a - u_{1s})/c$, $\nu_{1s} = [(b+1)u_{1s} - a]/u_{1s}^2$, and $u_{2s} = \{b + 1 \pm [(b+1)^2 - 4\nu_{2s} a]^{1/2}\}/(2\nu_{2s})$. The plus and minus signs in Eq. (22) correspond to the higher and lower steady states, respectively, in reactor 2. Note that the steady states are independent of r, since only Eq. (14′) depends on r, and this expression does not enter into the calculation of the SS's.

How many additional SS's, if any, occur depends in general upon the functions $f(u,\nu)$ and $g(u,\nu)$. Here we examine our coupled Brusselator system.

Considered as a function of u_1, Eq. (22) is a rather complex expression, the roots of which are the steady-state concentrations of u_1. In Fig. 3, we plot the quantity

$$H(u_1) = c(\nu_2 - \nu_1)/d + 2(a - u_1)(1/d + 1/k_1) \tag{23}$$

which has the same roots as Eq. (22) and where $\nu_1 = [(1+b)u_1 - a]/u_1^2$, and $\nu_2 = [(1+b)(2a - u_1) - a]/(2a - u_1)^2$. If $k_1 < k_{1-\mathrm{ST}}$, where ST stands for subcritical Turing, Eq. (22) has only the homogeneous root, $u_1 = a$ (curve 1). If $k_{1-\mathrm{ST}} < k_1 < k_{1-T}$, expression (22) has five positive roots,

and the steady state $u_{SS}=a$ is still stable (curves 2, 3). The smallest and largest roots (around 0.6 and 5.6, respectively) are also stable. These values approximate the minimum and maximum concentrations (u_{min} and u_{max}) of the Turing patterns in the full heterogeneous system (2)–(4) [see Fig. 5(c)] or in system A-I with small nonzero D_u [see curve 1 in Figs. 5(a) and 5(b)]. In both cases, the smallest root matches the minimum of the Turing patterns almost exactly, but the Turing maximum in system A-I is slightly smaller than the largest root due to "diffusive blurring." Note also that the roots in system B-I depend slightly on k_1 (see Fig. 3), while the maxima and minima of the Turing patterns must correspond to the wave number k at which Re(Λ) reaches its maximum. If $k_{1-T}<k_1$, expression (22) has three positive roots, and steady state $u_{SS}=a$ becomes unstable (curve 4). The value k_{1-T} found here as the transition from 5 to 3 solutions of the steady-state equations for system B coincides with the value k_{1-T} found earlier from linear stability analysis as the value for the onset of Turing instability in system A-I, a striking link between the continuous and discrete approaches. The region $k_{1-ST}<k_1<k_{1-T}$ is a region of bistability and corresponds to *subcritical* Turing structures, as will be shown later in simulations. If, in this range of k_1, the initial concentrations for subsystems 1 and 2 are chosen to correspond to the maximum and minimum roots ($u_1=u_{min}$ and $u_2=u_{max}$), the system persists unchanged in time.

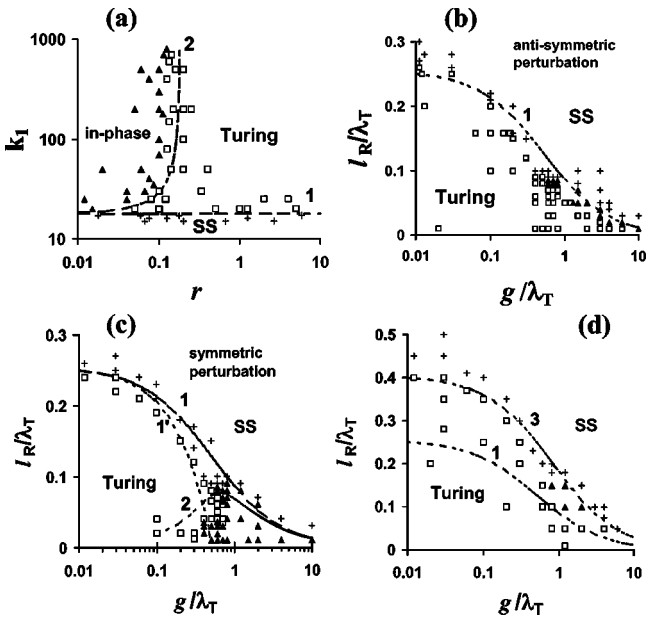

FIG. 4. Parametric diagrams. $a=3.06$, $b=7$, $c=2$, $d=5$. (a) System B-I. Horizontal line 1 between SS and Turing domain is $k_1=k_{1-T}$. Line 2 is $k_1=k_{1-cr}$. (b)–(d) Full system (2)–(4). Line 1′ is $(2l_R+g)/\lambda_T=0.5$; $\lambda_T=14.91$; line 1 is $(2l_R+g')/\lambda_T=p$, $p=0.5$; line 3 is the border for subcritical Turing bifurcation, $(2l_S+g')/\lambda_T=p=0.8$; line 2 is transformed line 2 in (a). □, Turing pattern; +, SS; ▲, in-phase oscillations. (b) and (c) correspond to initial antisymmetric and symmetric small perturbation of homogeneous steady state, respectively. In (d), initial pattern is a Turing pattern.

D. Numerical calculations: System B-I

To verify the results of the linear stability analysis, we integrated the ODE's for system B-I numerically at several k_1 and r for the Brusselator model. For integrating the ODE's and PDE's, we used the FlexPDE package.[23] In all cases, the initial concentrations (subscript 0) were chosen as the homogeneous steady state $\nu_{1-0}=\nu_{2-0}=\nu_{SS}=b/a$, and $w_{1-0}=w_{2-0}=w_{3-0}=w_{SS}=cb/(ad)$ with two types of small perturbation for the u variable: symmetric and antisymmetric. For symmetric perturbation, $u_{1-0}=u_{2-0}=u_{SS}(1+0.001)$, $u_{SS}=a$. For antisymmetric perturbation, $u_{1-0}=u_{SS}(1+0.001)$ and $u_{2-0}=u_{SS}(1-0.001)$. Results of these simulations are presented in Fig. 4(a). In the case of antisymmetric perturbation, the final pattern does not depend on r: if $k_1<k_{1-T}$ (curve 1), the final pattern is the homogeneous steady state, $u_1=u_2=u_{SS}$, $\nu_1=\nu_2=\nu_{SS}$, $w_1=w_2=w_3=w_{SS}$; if $k_{1-T}<k_1$, the final pattern is a new stationary "Turing" steady state, $u_1=u_{max}$, $u_2=u_{min}$, $\nu_2=\nu_{max}$, $\nu_1=\nu_{min}$. In the case of symmetric perturbation, the "Turing" domain is divided by a curve that approximately coincides with the function $k_{1-cr}(r)$ (curve 2). Below and to the right of this curve, we obtain stationary Turing patterns, while above and to the left we find in-phase oscillations with a time course like that found in the full system and shown in Fig. 5(d).

We conclude that the positive eigenvalue Re1 obtained from the first factor in Eq. (19), $(D_0-k_1D_1)=0$, is responsible for the growth of antisymmetric perturbations, while the second positive eigenvalue, Re2, obtained from $(2k_1rD_0+\Lambda D_0-\Lambda k_1D_1)=0$ controls the growth of symmetric perturbations.

There exists a critical value of c, $c_{cr}=a^2/(b-1)$ (in general, $c_{cr}=g_v-f_vg_u/f_u$), such that when $c<c_{cr}$, Re(Λ) is negative for any wave number k or coupling constant k_1 for systems A-I or B-I, respectively. Since Re1 is a monotonically increasing function of k_1, c_{cr} can be found by setting $D_1=0$, obtained from $D_0-k_1D_1=0$ as $k_1\to\infty$. When Re(Λ)<0, small perturbations of the homogeneous steady state must decay. However, examination of system B-I, reveals that this system has five steady states (three stable and two unstable) at $c<c_{cr}$ and $k_1>k_{1-ST}$. A further increase in k_1 does not lead to transition from five roots to three, i.e., to supercritical Turing bifurcation, as occurs in the case shown in Fig. 3, where $c>c_{cr}$. This result implies that subcritical Turing bifurcation can be found not only for system B-I, but also for system A-I when $c<c_{cr}$, since both systems represent the same heterogeneous spatially extended system (2)–(4). To demonstrate this phenomenon numerically, we choose $D_u=0.1$ instead of $D_u=0$ [see Fig. 2(a)], since the plateau in Re(Λ) in the latter case leads to special Turing patterns without a characteristic wavelength and causes the system to "remember" any initial perturbations in the form of stationary clusters. The results of our simulations of subcritical Turing patterns are presented in Figs. 5(a) and 5(b). To our knowledge, subcritical Turing bifurcation in chemical systems has been found only in the Lengyel–Epstein model[24] and was explained in that system by solving a set of amplitude equations.[25] Here we present another example of subcritical Turing instability in a chemically plausible system and give a simple explanation based on analysis of the steady states of coupled subsystems.

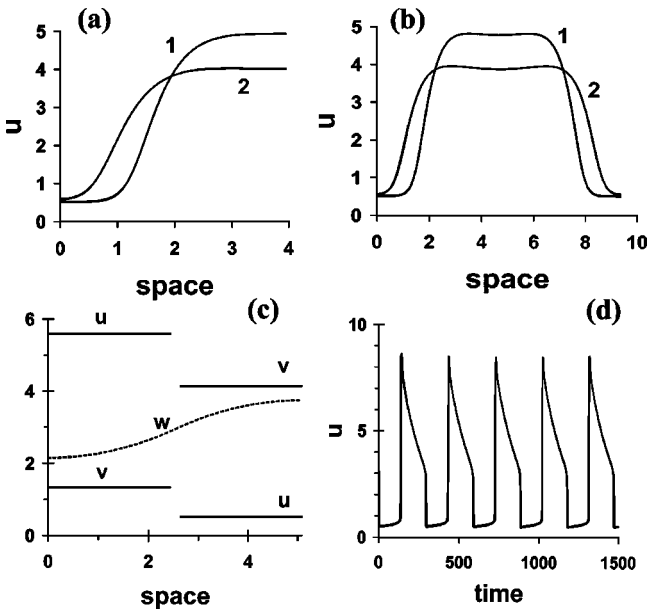

FIG. 5. Modes $m=1$ (a) and $m=2$ (b) of subcritical Turing patterns in system A-I. $c=$(curve 1) 2, (curve 2) 1.5, $[c_{cr}=a^2/(b-1)=1.5606]$; $D_u=0.1$; $D_v=0$, $L/\lambda_T=$(a) 0.2786, (b) 0.66; $\lambda_T=14.156=2\pi/k_T$, $k=k_T$ when $\mathrm{Re}(\lambda)=0$. $\mathrm{Re}(\Lambda)$ has a positive maximum at $k_0=0.810\,55$ for $c=2$ (curve 1). $\mathrm{Re}(\Lambda)<0$ at any wave number k for $c=1.5$ (curve 2). Concentration profile of curve 1 was taken as initial pattern that resulted in curve 2. For parameters of curve 2, small initial perturbation of the homogeneous steady-state decays. (c) Turing pattern for full heterogeneous system (2)–(4). $r=0.01$, $l_R/\lambda_T=0.165$; $\lambda_T=14.91$; $L=5.0856$. $D_u=D_v=D_w=100$ in the reactors and $D_u=D_v=0$ and $D_w=100$ in the gap; $c=2$, curve "w" is $10(w-0.8)$. (d) oscillations of u at $l_R/\lambda_T=0.01$ and $g/\lambda_T=10$. Period of oscillation varies with l_R and g. In all frames, $a=3.06$, $b=7$, $d=5$, $D_w=100$.

E. Numerical simulations and approximate analytic results: Full system

The above analysis affords several insights into how the full heterogeneous system shown in Fig. 1 can behave. In particular, we expect it to exhibit homogeneous SS, super- and subcritical Turing patterns, and in-phase oscillations, depending on the parameters and initial conditions. Here we explore the effects of geometry by independently varying the lengths of the reactor l_R and the gap g. We simulate the full Eqs. (2)–(4) with $D_u=D_v=D_w$ in the two reactors and $D_u=D_v=a=b=c=d=u=\nu=0$ in the gap. The results of our simulations are shown in Figs. 4(b)–4(d). For small antisymmetric perturbations of the initially homogeneous steady state, most geometries lead to either Turing patterns or the original steady state. A small domain of in-phase oscillation is found along the boundary between the SS and Turing domains at relatively large g and small l_R. Examples of Turing patterns and in-phase oscillations are shown in Figs. 5(c) and 5(d), respectively.

We now seek to utilize our analysis of systems A-I and B-I to find an analytical expression for the boundary between the SS and Turing domains in the full heterogeneous system. In the homogeneous approximation, setting $\mathrm{Re}(\Lambda)=0$ for mode $m=1$, gives

$$L/\lambda_T=p=0.5 \tag{24}$$

at the onset of Turing instability [see Fig. 2(b)]. In the actual system, $L=2l_R+g$, which, combined with Eq. (24), gives curve $1'$ in Fig. 4(c). We observe that this expression accurately represents the boundary between SS and Turing patterns only for small g and large l_R. To obtain a better expression for the boundary, we should take into account that the length in Eq. (24) is that of the homogeneous system that best approximates the full heterogeneous system, i.e., system A-I, which is not necessarily identical to L. We write instead of Eq. (24)

$$L'/\lambda_T=p=0.5. \tag{25}$$

Our analysis of system A-I implies that, for the mode $m=1$ to persist, L' should be less than or equal to $\lambda_T/2$. Figure 4(b) shows, however, that Turing patterns are found in the full system for $g>\lambda_T$. How can the length L' for the homogeneous approximation be expressed in terms of the actual g? For very small gaps ($g\ll\lambda_T$), the difference between the homogeneous approximation and the full heterogeneous system should be negligible, and we should have $L'=L$. As the gap grows, we must have $L'<p\lambda_T$ for any values of g and l_R in order for the $m=1$ Turing pattern to occur. A simple, smooth function of g that satisfies these conditions is

$$g'=p\lambda_T g/(p\lambda_T+g) \tag{26}$$

which can be considered as the effective gap length of system A-I. We then write

$$L'=2l_R+g'=2l_R+p\lambda_T g/(p\lambda_T+g)=p\lambda_T. \tag{27}$$

Expression (27), shown as curve 1 in Figs. 4(b)–4(d), affords a much more satisfactory description of the boundary between the SS and Turing domains.

With symmetric perturbation [Fig. 4(c)], the domain of in-phase oscillation is significantly larger. To find the line separating the Turing and in-phase oscillation domains in the full system, we combine the results obtained in the coupled reactor approximation (system B-I) shown in Fig. 4(a) and the Turing wavelength obtained in the spatially extended homogeneous system A-I. We seek an expression that corresponds to curve 2 in Fig. 4(a) for $k_{1-\mathrm{cr}}$, but now in the (g,l_R) parameter plane. To translate $k_{1-\mathrm{cr}}$ from the (r,k_1) to the (g,l_R) plane, we focus on the $m=1$ mode, where $k=\pi/L'$ and introduce Eq. (27) into Eq. (20) to obtain

$$k_1=\pi^2 D_w/L'^2=\pi^2 D_w/(2l_R+g')^2. \tag{28}$$

Using Eq. (26) and replacing l_R by rg in Eq. (28) yields a quadratic equation in g, which may be solved for $g(r,k_1)$ and hence $l_R(r,k_1)$, allowing us to perform the desired transformation of the $k_{1-\mathrm{cr}}$ curve. The result is shown as curve 2 in Fig. 4(c).

The in-phase oscillations found in our full heterogeneous system do not emerge from analysis of system A-I, but can be understood from the behavior of system B-I. In-phase oscillations are found when the gap is large, which is equivalent to a long time delay for the "coupled reactors." Interestingly, the resulting oscillations [Fig. 5(d)] are strongly relaxational, resembling periodic switching between two steady states, which correspond to the two new SS's of the

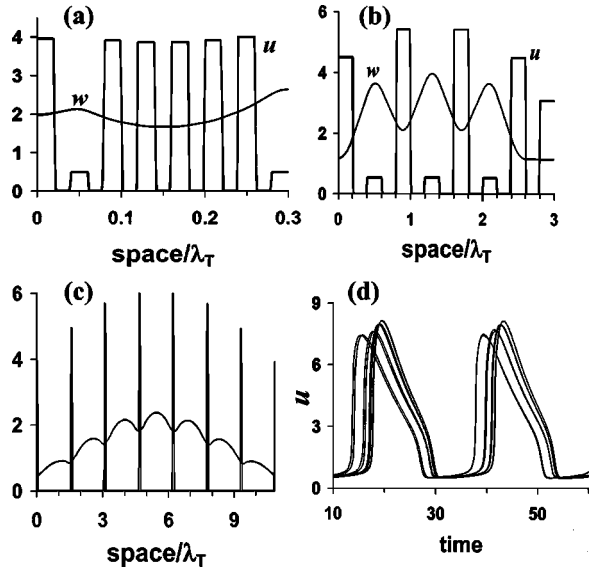

FIG. 6. Stationary Turing structures [(a) and (b)] and in-phase oscillations [(c) and (d)] for eight coupled in-line microreactors with length l_R separated by identical gaps. $l_R/\lambda_T = g/\lambda_T =$ (a) 0.02, (b) 0.2; for (c) and (d) $l_R/\lambda_T = 0.05$, $g/\lambda_T = 1.5$. (d) time series of u recorded at centers of all eight reactors. (c) is a snapshot at a single instant; sharp peaks are u; smooth, continuous curve is $10(w-0.8)$.

coupled system. The uncoupled Brusselator model is quite ''soft'' and yields sinusoidal-like rather than relaxation-type oscillations.

The subcritical Turing instability found in our approximations also arises in the full system. If we take the Turing pattern as the initial condition, we find a significant enlargement of its domain of stability [Fig. 4(d)]. In particular, Turing patterns remain stable even for values of $2l_R$ greater than the stability limit $\lambda_T/2$ obtained from the linear stability analysis. The subcritical Turing domain lies between curves 1 and 3 in Fig. 4(d). Small initial perturbations to the homogeneous steady state decay in this region, while superthreshold perturbations cause a transition to the Turing pattern. Note that, in contrast to previous work, the subcriticality of Turing patterns is obtained here by varying the system length, rather than the kinetic parameters or the diffusion coefficients.

To find an analytical expression for curve 3, which marks the boundary of the subcritical Turing region in Fig. 4(d), we replace $k_{1-T}(=17.77)$ by the value $k_{1-ST}(=7.05)$ found above and set $p=0.5\times(k_{1-T}/k_{1-ST})^{1/2}$ in Eqs. (25) or (27).

F. Several microreactors

We also performed simulations over a range of parameter values for a system consisting of several identical microreactors separated by identical gaps. The boundaries between regions seen in Fig. 4 change very little, though the Turing domain expands slightly at the expense of the SS domain. If l_R and g are sufficiently smaller than λ_T, a group of neighboring reactors can have identical states [Fig. 6(a)]. This effect is caused by the fact that the signaling species w, which diffuses throughout the system, aspires to have a concentration profile with wavelength λ_T. To do so, it must vary on a length scale that encompasses several adjacent microreactors. If L is close to λ_T, we obtain a Turing pattern in which adjacent microreactors are in opposite stationary states [Fig. 6(b)]. A domain of in-phase oscillations is also found for this system of multiple coupled microreactors [Figs. 6(c) and 6(d)].

III. COUPLING THROUGH THE ACTIVATOR: WAVE INSTABILITY

In this section we consider a system with the geometry shown in Fig. 1, in which the signaling variable w is linearly coupled with the activator u. The general form of such a system is

$$\partial u/\partial t = f(u,\nu) - cu + dw + D_u \partial^2 u/\partial x^2, \tag{29}$$

$$\partial \nu/\partial t = g(u,\nu) + D_v \partial^2 \nu/\partial x^2, \tag{30}$$

$$\partial w/\partial t = cu - dw + D_w \partial^2 w/\partial x^2, \tag{31}$$

where $D_u = D_v = D_w$ in the reactors, and $D_u = D_v = u = \nu = 0$ in the gap.

Since, as we show below, this system generates out-of-phase oscillations, we very briefly review rhythmogenesis of out-of-phase oscillations. The first attempt to generate out-of-phase oscillations, in the so-called ''echo'' regime, where two cells are excited in turn, was made by Krinsky *et al.*[14] with a strongly relaxational system (FitzHugh–Nagumo-type model). Although they obtained several pulses, the oscillations were not stable and soon died out. Tyson[26] successfully generated echo waves in the Oregonator model of the Belousov–Zhabotinsky reaction by coupling the activator variables in two identical reactors. For very narrow ranges of the time-scale factor ε, the coupling strength, and the initial conditions, he obtained stable out-of-phase oscillations, which coexisted with in-phase damped oscillations and the homogeneous steady-state solution for other initial conditions. The excitability of the system and its strong relaxational character (smallness of ε) were essential for the out-of-phase oscillations. Below we show that system (29)–(31) can generate out-of-phase oscillations for any initial conditions as a result of the wave instability.

A. Linear stability analysis: PDE's for system A-II and ODE's for system B-II

Using the same approach as in Sec. II, we can explore a homogeneous approximation, system A-II (the analog of system A-I, but with coupling through the activator), with $D_u = D_v = 0$ and $D_w \neq 0$ for preliminary analysis of the wave properties of the full heterogeneous system (29)–(31) that has $D_u = D_v = D_w \neq 0$ in the reactors. The characteristic equation for the eigenvalues of the linearized system A-II is

$$\begin{vmatrix} f_u - c - \Lambda & f_v & d \\ g_u & g_v - \Lambda & 0 \\ c & 0 & -d - \Lambda - k^2 D_w \end{vmatrix} = M_0 - k^2 D_w M_1 = 0, \tag{32}$$

where

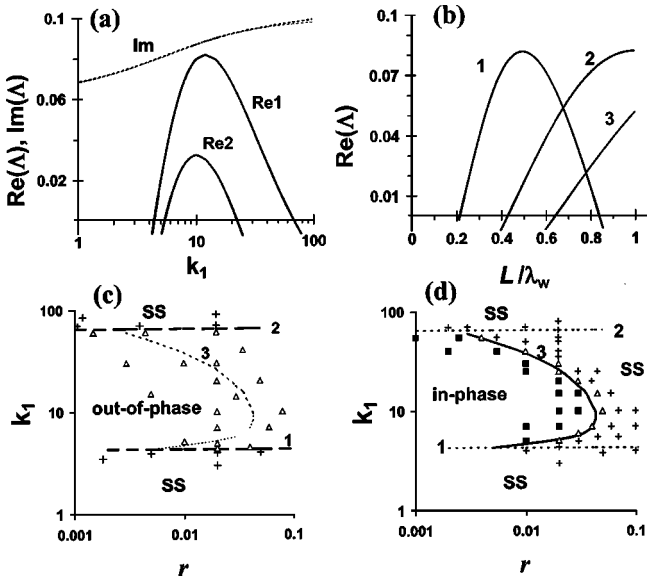

FIG. 7. (a) Dispersion relations for systems A-II and B-II ($k_1=k^2D_w$). Brusselator parameters: $a=2.85$, $b=11$, $c=2$, $d=5$; $D_u=D_v=0$, $D_w=100$; $r=0.025$. lm1 and lm2 are almost identical; shown is ''Im'' =Im2/50. (b) System A-II. Transformed curve Re1 ($k=m\pi/L$) for wave modes $m=1$, 2, and 3. $\lambda_w=2\pi/k_0=17.923$, where k_0 corresponds to the maximum of curve Re1 in (a), with $k=(k_1/D_w)^{1/2}$. For $m=1$, $(L/\lambda_w)_{\min}=0.22$, $(L/\lambda_w)_{\max}=0.84$. Maximum of curve 2 is at $L=\lambda_w$. (c) and (d) Parametric diagrams for system B-II in the k_1-r plane for (c) antisymmetric and (d) symmetric perturbations of the homogeneous steady state. $(k_1)_{\min}=4.3$ (line 1), $(k_1)_{\max}=65$ (line 2) [values of k_1 at which Re $1=0$ in (a)]. Curve 3 shows k_1 at which Re $2=0$. Δ, out-of phase oscillations; ■, in-phase oscillations; +, steady state (SS).

$$M_0=(f_u-c-\Lambda)(g_v-\Lambda)(-d-\Lambda) - cd(g_v-\Lambda)-f_vg_u(-d-\Lambda), \tag{33}$$

$$M_1=(f_u-c-\Lambda)(g_v-\Lambda)-f_vg_u. \tag{34}$$

Proceeding as in Sec. II, we can also construct a coupled reactor approximation, which yields the characteristic equation for system B-II (see next section):

$$(M_0-k_1M_1)(2k_1rM_0+\Lambda M_0-\Lambda k_1M_1)=0 \tag{35}$$

and Eq. (20) again relates the wave number of the pattern formation approach to the coupling constant in the coupled reactor approximation.

Dispersion curves calculated from Eq. (35) with the Brusselator model are shown in Fig. 7. Curves Re1 and Re2 correspond to the most positive eigenvalues obtained from the first and second factors, respectively, in Eq. (35). Both eigenvalues have nonzero imaginary parts when $\mathrm{Re}(\Lambda)>0$, which implies that the system has a wave instability. We denote the zeroes of Re1, which is independent of r, by $(k_1)_{\min}$ and $(k_1)_{\max}$. The zeros of Re2 tend to $(k_1)_{\min}$ and $(k_1)_{\max}$ as $r\to 0$. As r increases, the maximum of curve Re2 decreases and reaches 0 at some critical value. The dependence of the zeros of Re2 on r is shown in Figs. 7(c) and 7(d) as curve 3.

The wave properties of system A-II are depicted in Fig. 7(b), which shows the transformed ($k=m\pi/L$) curve Re1 from Fig. 7(a) for several wave modes m. The characteristic wavelength λ_w is given by $2\pi/k_0$, where $k_0=(D_w/k_{1-0})^{1/2}$ and k_{1-0} corresponds to the maximum of curve Re1. For two coupled small reactors we expect to find only the $m=1$ (half wavelength) mode; therefore we focus on curve 1 and its zeros. If $L<L_{\min}$, at which $\mathrm{Re}(\lambda)=0$ for $m=1$ ($L_{\min}/\lambda_w=0.22$), no oscillations are possible.

B. Steady states: System B-II

The equations for system B-II are

$$du_i/dt=f(u_i,\nu_i)-cu_i+dw_i, \tag{36}$$

$$d\nu_i/dt=g(u_i,\nu_i), \tag{37}$$

$$dw_i/dt=cu_i-dw_i-k_1(w_i-w_3), \tag{38}$$

$$dw_3/dt=-k_1r(2w_3-w_1-w_2), \tag{14'}$$

where $i=1$, 2. By an algorithm analogous to that employed in Sec. II [Eq. (21)], the steady states of system B-II are found from

$$f(u_{1s},\nu_{1s})=-f(u_{2s},\nu_{2s}) \tag{39}$$

by solving $g(u,\nu)=0$ for the u_{is} in terms of the ν_{is} and then solving

$$u_{2s}=u_{1s}-2(1+d/k_1)f(u_{1s},\nu_{1s})/c$$

and substituting it into Eq. (39). For the Brusselator model, Eq. (39) yields

$$a-u_1=-(1+d/k_1)(a-u_1)/c \tag{40}$$

which has only one root, $u_1=a=u_2$. Note that the analogous Eq. (22) may have up to five roots. More generally, we expect that in systems similar to the Brusselator, like the Oregonator or the Lengyel–Epstein model, where the activator kinetics are highly nonlinear and the inhibitior kinetics are (nearly) linear, coupling through the activator will not generate additional roots.

C. Numerical calculations: ODE's for system B-II

Though, as was the case in Fig. 2(a), the simple linear stability analysis applied here does not differentiate between anti-symmetric and symmetric perturbations, curves Re1 and Re2 in Fig. 7(a) enable us to distinguish between different symmetric perturbations of the homogeneous steady state. In our simulations, we therefore applied both types of perturbations as we did in Sec. II. Figures 7(c) and 7(d) show parametric diagrams for antisymmetric and symmetric perturbations, respectively. Curves 1 and 2 correspond to $(k_1)_{\min}$ and $(k_1)_{\max}$, respectively. When k_1 lies between these values at any r, antisymmetric perturbation always produces out-of-phase oscillations in system B-II. For symmetric perturbations, in-phase oscillations occur for those k_1 and r for which $\mathrm{Re}\,2>0$ [points between curves 1 and 2 and to the left of curve 3 in Fig. 7(d)]. In a small neighborhood of curve 3, out-of-phase oscillations were found. For all other points in the $r-k_1$ plane, system B-II generates homogeneous steady states.

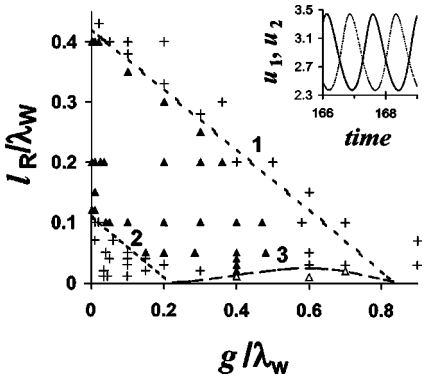

FIG. 8. Parametric diagram for full system (29)–(31). All oscillations (filled triangles) are out of phase for both symmetric and antisymmetric perturbation, + indicates SS. Open triangles mark transient in-phase oscillations for symmetrical initial perturbation, which decay into out-of-phase oscillations. $L/\lambda_w = 0.84$ for line 1 and 0.22 for line 2. Curve 3 corresponds to curve 3 in Figs. 7(c) and 7(d). Inset: typical out-of-phase oscillations at $l_R/\lambda_w = 0.3$ and $g/\lambda_w = 0.01$; u_1 and u_2 are concentrations of u at the centers of left and right reactors, which are nearly homogeneous.

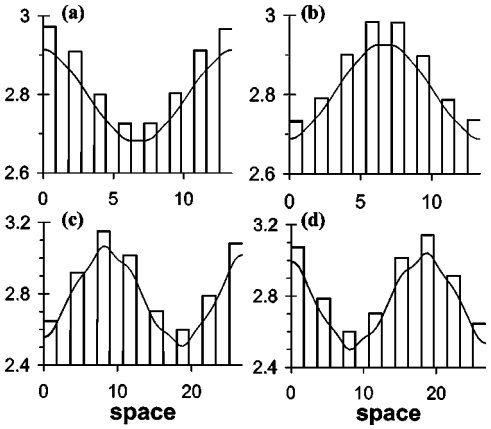

FIG. 9. Examples of standing waves for eight coupled in-line reactors with total length $L = 8l_R + 7g =$ (a) and (b) $0.75\lambda_w$, (c) and (d) $1.5\lambda_w$ at $l_R = g =$ (a) and (b) $0.05\lambda_w$, (c) and (d) $0.1\lambda_w$. Snapshot pairs (a)–(b) and (c)–(d) are separated in time by $T/2$, where $T = 1.38$ is the period of oscillation. Smooth curve is $20(w-1)$; histograms show u.

D. Numerical calculations: PDE's for full system (29)–(31)

The results of our simulations of the full system, varying l_R and g, are shown in Fig. 8. For both symmetric and antisymmetric perturbations, the only stable, nonstationary behavior we observe consists of out-of-phase oscillations. These occur between curves 1 and 2, which correspond to $L_{\min}$ and $L_{\max}$, the zeroes of $\mathrm{Re}(\Lambda)$ on curve 1 in Fig. 7(b). For small l_R and large g, the domain of oscillations is narrower then the distance between curves 1 and 2. Remnants of the in-phase oscillations found for symmetrical perturbation of system B-II [Fig. 7(d)] can be seen below curve 3, which corresponds to curve 3 of Figs. 7(c) and 7(d). In this domain, symmetric perturbation generates long-lasting, transient, in-phase oscillations (tens of oscillation periods), which slowly transform into out-of-phase oscillations. A typical example of out-of-phase oscillations is shown in the inset of Fig. 8. These soft, nearly sinusoidal oscillations are in striking contrast to the relaxationlike oscillations seen in Fig. 5(d) for the case of coupling through the inhibitor.

E. Several microreactors

Simulations performed for a system of several identical reactors separated by identical gaps (Fig. 9) demonstrate that the wave properties of the entire system control the behavior. When $L = 0.75\lambda_w$, where mode $m = 2$ possesses the largest $\mathrm{Re}(\Lambda)$ [Fig. 7(b)], we obtain standing waves with $m = 2$ [one wavelength, Figs. 9(a) and 9(b)]. When $L = 1.5\lambda_w$, mode $m = 3$ dominates, and we see standing waves with one and a half wavelengths [Figs. 9(c) and 9(d)].

IV. DISCUSSION AND CONCLUSION

We have developed here a general approach for studying heterogeneous systems consisting of ''active'' droplets, in which we employ both continuous (PDE) and discrete (ODE) approximate descriptions of the system. Starting from subsystems that each have only a single stable steady state, we showed that by varying the total system length L (e.g., by changing the size of the gap between droplets), which for a given mode is equivalent to variation of the wave number k, we could cause the real part of an eigenvalue of the Jacobian matrix to become positive, thereby leading to a new system behavior: Turing patterns, in-phase oscillations, or wave instability.

Experiments in which micro-oscillators are coupled have been conducted with the aid of cation-exchange beads loaded with a catalyst for the BZ reaction.[27,28] In these experiments, both activator and inhibitor were able to diffuse between beads. Coupling experiments with macroscopic BZ reactors, with all species coupled and nearly identical feed concentrations, yielded in-phase and out-of-phase oscillations as well as inhomogeneous (Turing) steady states and ranges of bistability among these dynamical states.[29] In our experiments with the BZ-AOT system,[1–3] mass exchange between nanodroplets also leads to diffusion of the activator and inhibitor throughout the medium, but their diffusion coefficients are much smaller than that of the signaling species diffusing directly through the oil phase. Small water droplets in an oil phase, produced by microfluidic devices in microchannels,[30] would provide an attractive system to test our predictions experimentally.[31,32] Living cells or microorganisms may also offer such an opportunity.[33]

The existence of a subcritical Turing bifurcation has implications for the velocity of fronts in systems of this type. In calculating the front velocity of expanding Turing patterns in the Lengyel–Epstein model, Jensen *et al.*[34] showed that values obtained from direct simulations of PDE's differed significantly from those given by the theory developed by Ben-Jacob *et al.*[35] and van Saarloos[36,37] in the range of parameter b where subcritical Turing bifurcation occurs. If the subcritical region corresponds to bistability between different stable steady states separated by an unstable one, as we have argued here, then application of the theory, which assumes fronts propagating between an unstable steady state and a stable one cannot give correct results.

We are aware of only one mechanism in the liter-

ature[38,39] that leads to nonequilibrium dynamical patterns with submicron or even nanometer wavelengths $\lambda = (r_0 l_D)^{1/2}$ much shorter then the diffusion length $l_D = (D\tau)^{1/2}$, where r_0 is the radius of a thermodynamically stable nanostructure, like water nanodroplets (micelles) or other molecular clusters.[40] The mechanism explored here suggests that if we have a thermodynamically stable structure (e.g., two droplets with a gap, as in Fig. 1) even with very short total length ($L \ll l_D$), a nonequilibrium Turing pattern (half wavelength, mode $m=1$) can develop within this structure. As we suggest above, such structures can be created with microfluidic devices, or in water-in-oil-in-water droplets,[30–32,41] or even found in living cells.

Note that the wavelength of the Turing pattern that actually develops in two isolated coupled drops depends on the total length L of the system and can be either significantly smaller than the intrinsic Turing wavelength λ_T or larger than λ_T [for a large gap, shown in Figs. 4(b)–4(d)]. The existence of very small Turing wavelengths results from the plateau in the dispersion curves as $k \to \infty$ [curve Re1 in Fig. 2(a)]. The dependence of the Turing wavelength on the system geometry in this heterogeneous system differs from the geometry independence of the intrinsic Turing wavelength found in homogeneous systems.

If the diffusion coefficients of the species inside a single droplet differ significantly, for example, in an AOT microemulsion loaded with the BZ system,[1–3] where, with appropriate scaling, $D_v \approx D_u = 1$, $D_w \approx 100$, and we have wave instability with a dispersion curve like Re1 in Fig. 7(a), the behavior of a single droplet with nonzero flux boundary conditions (e.g., in a large medium where only w can diffuse) may depend on its size l_R, even when $l_R \ll \lambda_w$ when $\mathrm{Re}(\Lambda) < 0$. Since w outside the droplet is approximately constant, we may assume that at the droplet's boundary $w = w_{SS}$, and Eqs. (29)–(31) at the boundary become

$$du/dt = f(u,v) - cu + dw_{ss}, \tag{29s}$$

$$dv/dt = g(u,v). \tag{30s}$$

For some system parameters (e.g., the Brusselator with $a = 2.81$, $b=11$, $c=2$, $d=5$, and $w_{SS} = ac/d$), Eqs. (29s) and (30s) may give rise to oscillations, with $\mathrm{Re}(\Lambda) > 0$ at $k=0$. Thus the boundary may serve as a source of oscillations. At large surface to volume ratios, this phenomenon may lead to bulk oscillations in the droplet at small $l_R (< \lambda_w/100)$, while for larger l_R (but smaller than $(l_R)_{\min}$, at which $\mathrm{Re}(\Lambda)=0$), the droplet remains in the steady state, as the boundary effect is insufficient to dominate in the droplet bulk. We have verified this result by direct simulations without assuming that $w = w_{SS}$ at the droplet boundary.

The accuracy of the homogeneous approximation, system A, increases as the ratio $r\ (= l_R/g)$ increases, while the coupled reactor approximation, system B, becomes more appropriate as $r \to 0$. Both approximations yield insights into the properties of the full heterogeneous system shown in Fig. 1 and allow us to bring together the languages of "pattern formation" and "coupled oscillators." For example, we have pointed out the correspondence between the inhomogeneous steady states of two coupled reactors and Turing patterns in a homogeneous system and have shown that the Turing maxima and minima are well approximated by these steady states. The out-of-phase oscillations found in "coupled oscillators" are equivalent to a wave instability in the "pattern formation" formulation. The coupling strength k_1 in the former approach is related by Eq. (20) to the wave number k of the latter. Heterogeneous systems, in which both the activator and inhibitor in subsystems are coupled through messenger molecules, should be capable of displaying even more complex behavior than we have described here. While it should be possible to design microfluidic chemical systems that display the behavior predicted in this work, these ideas may have their most important applications to morphogenesis and the dynamics of microorganisms.

ACKNOWLEDGMENTS

This work was supported by a grant from the National Science Foundation. We thank Anatol Zhabotinsky for helpful discussions.

[1] V. K. Vanag and I. R. Epstein, Phys. Rev. Lett. **87**, 228301 (2001).
[2] V. K. Vanag and I. R. Epstein, Science **294**, 835 (2001).
[3] V. K. Vanag and I. R. Epstein, Phys. Rev. Lett. **88**, 088303 (2002).
[4] A. M. Turing, Philos. Trans. R. Soc. London, Ser. B **237**, 37 (1952).
[5] V. K. Vanag and I. R. Epstein, J. Phys. Chem. A **106**, 11394 (2002).
[6] M. Dolnik, A. M. Zhabotinsky, and I. R. Epstein, Phys. Rev. E **63**, 026101 (2001).
[7] S. Smale, in *Lectures on Mathematics in the Life Science*, edited by J. D. Cowan (American Mathematical Society, Providence, Rhode Island, 1974), Vol. 6, pp. 15–26.
[8] Q. Ouyang and H. L. Swinney, Nature (London) **352**, 610 (1991).
[9] R. Herrero, M. Figueras, J. Rius, F. Pi, and G. Orriols, Phys. Rev. Lett. **84**, 5312 (2000).
[10] D. V. Ramana Reddy, A. Sen, and G. L. Johnston, Phys. Rev. Lett. **80**, 5109 (1998).
[11] D. V. Ramana Reddy, A. Sen, and G. L. Johnston, Phys. Rev. Lett. **85**, 3381 (2000).
[12] R. Holz and F. W. Schneider, J. Phys. Chem. **97**, 12239 (1993).
[13] J. Weiner, R. Holz, F. W. Schneider, and K. Bar-Eli, J. Phys. Chem. **96**, 8915 (1992).
[14] V. I. Krinsky, A. M. Pertsov, and A. N. Reshetilov, Biofizika **17**, 271 (1972).
[15] M. Dolnik, J. Kosek, V. Votrubova, and M. Marek, J. Phys. Chem. **98**, 3707 (1994).
[16] M. N. Stolyarov, V. A. Romanov, and E. I. Volkov, Phys. Rev. E **54**, 163 (1996).
[17] G. Nicolis and I. Prigogine, *Self-Organization in Nonequilibrium Systems* (Wiley-Interscience, New York, 1977).
[18] I. Lengyel and I. R. Epstein, Science **251**, 650 (1991).
[19] J. J. Tyson and P. C. Fife, J. Chem. Phys. **73**, 2224 (1980).
[20] P. Andersen, M. Bache, G. Dewel, and P. Borckmans, Phys. Rev. E **60**, 297 (1999).
[21] A. B. Rovinsky and M. Menzinger, Phys. Rev. Lett. **69**, 1193 (1992).
[22] J. A. Vastano, J. E. Pearson, W. Horsthemke, and H. L. Swinney, Phys. Lett. A **124**, 320 (1987).
[23] FlexPDE, http://www.pdesolutions.com/flexpde.htm
[24] O. Jensen, V. O. Pannbacker, G. Dewel, and P. Borckmans, Phys. Lett. A **179**, 91 (1993).
[25] P. Borckmans, G. Dewel, A. De Wit, *et al.*, Int. J. Bifurcation Chaos Appl. Sci. Eng. **12**, 2307 (2002).
[26] J. J. Tyson, Ann. N.Y. Acad. Sci. **316**, 279 (1979).
[27] K. Miyakawa, T. Okabe, M. Mizoguchi, and F. Sakamoto, J. Chem. Phys. **103**, 9621 (1995).
[28] K. Miyakawa, T. Okabe, and F. Sakamoto, Phys. Rev. E **55**, 2005 (1997).
[29] M. F. Crowley and I. R. Epstein, J. Phys. Chem. **93**, 2496 (1989).
[30] S. L. Anna, N. Bontoux, and H. A. Stone, Appl. Phys. Lett. **82**, 364 (2003).
[31] I. G. Loscertales, A. Barrero, I. Guerrero, R. Cortijo, M. Marquez, and A. M. Ganan-Calvo, Science **295**, 1695 (2002).

[32] T. Thorsen, R. W. Roberts, F. H. Arnold, and S. R. Quake, Phys. Rev. Lett. **86**, 4163 (2001).
[33] E. Ben-Jacob, I. Cohen, and H. Levine, Adv. Phys. **49**, 395 (2000).
[34] O. Jensen, V. O. Pannbacker, E. Mosekilde, G. Dewel, and P. Borckmans, Phys. Rev. E **50**, 736 (1994).
[35] E. Ben-Jacob, H. Brand, G. Dee, L. Kramer, and J. S. Langer, Physica D **14**, 348 (1985).
[36] W. van Saarloos, Phys. Rev. A **37**, 211 (1988).
[37] W. van Saarloos, Phys. Rev. A **39**, 6367 (1989).
[38] M. Hildebrand, A. S. Mikhailov, and G. Ertl, Phys. Rev. E **58**, 5483 (1998).
[39] M. Hildebrand, M. Kuperman, H. Wio, A. S. Mikhailov, and G. Ertl, Phys. Rev. Lett. **83**, 1475 (1999).
[40] A. S. Mikhailov and G. Ertl, Science **272**, 1596 (1996).
[41] C. H. Villa, L. B. Lawson, L. Yimin, and K. D. Papadopoulos, Langmuir **19**, 244 (2003).